Designing Nanotextured Vanadium Oxide-Based Macroscopic Fibers: Application as Alcoholic Sensors

Céline M. Leroy,[†] Marie-France Achard,[†] Odile Babot,[‡] Nathalie Steunou,[§] Pascal Massé,[†] Jacques Livage,[§] Laurent Binet,[§] Nicolas Brun,[†] and Rénal Backov*[,†]

Centre de Recherche Paul Pascal, UPR 8641-CNRS, 115 Avenue Albert Schweitzer, 33600 Pessac, France, Institut des Sciences Moléculaires (ISM), UMR-5082 CNRS, Université Bordeaux-I, 351 cours de la libération, 33045 Talence Cedex, France, and Laboratoire de Chimie de la Matiére Condensée, UMR-7574 CNRS, 4 Place Jussieu, Université Pierre et Marie Curie, France

Received May 3, 2007

Composite vanadium oxide/PVA/latex macroscopic fibers have been generated by using an extrusion process. Specifically, inorganic vanadium oxide fibers enable the detection of 0.1 ppm of ethanol within 3−5 s at 42 °C, which is certainly one of the highest sensitivities to date concerning alcohol sensors. More importantly, by varying the starting latex inclusion contents, the shear rates applied during the extrusion process, and the final appliance of a thermal treatment, we were able to segregate each parameter involved within the mechanical and sensing properties associated with these as-synthesized fibers, i.e., the amount of the organic insulator counterpart, the degree of vanadium oxide ribbons alignment, and the induced porosity reached upon latex removal. Overall, we found out that all the parameters described above and involved within the as-synthesized fibers' mechanical and sensing properties are acting within a partitive action mode rather than a cooperative one.

Introduction

Syntheses over "all length scales"[1] and/or bioinspired approaches[2] were proposed around 10 years ago by Ozin and Mann, respectively, to promote complex and multiscale architectures. To reach such complex architectures with an idea of "rational design" it seems important to combine several domains of research, i.e., chemistry (inorganic, organic, polymeric, and hybrid), biology, physical chemistry of complex fluids. From this transdisciplinary approach has emerged a new transversal concept of "integrative chemistry",[3] offering thus a versatile tool box where the communities mentioned above will find specific items to compose their own synthetic pathway to reach specific functionalities occurring at diverse length scales. Integrative chemistry has been already applied by combining general chemistry with foams,[4] emulsions,[5] lyotropic mesophases,[6] biologic polymer,[7] three-dimensional colloid opal-like textures,[8] and so forth. To the previous set of texturing modes that mostly regard the areas of either soft matter, biology, or supramolecular chemistry we might associate inorganic polymerization occurring under mild or soft conditions. At that stage, "soft chemistry",[9] and more precisely the sol−gel process,[10] appears as the inorganic chemistry candidate of choice to both promote the inorganic connectivity while not destroying either the supramolecular template used at the mesoscale or the metastable thermodynamic systems imposed at the macroscopic length scale. Among inorganic oxide polymers obtained through the use of the sol−gel chemistry, vanadium oxide is of strong interest, as it is associated with a wide scope of applications ranging from catalysis to photochromism and more.[11] Gels of vanadium oxide can be obtained from sodium metavanadate as inorganic precursor and upon an ion exchange process. The texture of the resulting gels is made of vanadium oxide nanoribbon subunits that depict strong anisotropy[12,10b] and allows generating a inorganic liquid crystal associated with a nematic character.[13] We first took benefit of this textural property by aligning the ribbon subunits with the use of an extrusion process, thus

* Corresponding author. Phone: 33 (0)5 56 84 56 30. Fax: 33 (0)5 56 84 56 00. E-mail: backov@crpp-bordeaux.cnrs.fr.
† Centre de Recherche Paul Pascal.
‡ Université Bordeaux-I.
§ Université Pierre et Marie Curie.

(1) (a) Yang, H.; Kuperman, A.; Coombs, N.; Mamiche-Afara, S.; Ozin, G. A. *Nature* **1996**, 379, 703. (b) Feng, P.; Bu, X.; Stucky, G. D.; Pine, D. J. *J. Am. Chem. Soc.* **2000**, *5*, 994.
(2) (a) Mann, S. *Nature* **1988**, 332, 119. (b) Archibald, D. D.; Mann, S. *Nature* **1993**, *364*, 430.
(3) Backov, R. *Soft Matter* **2006**, *2*, 452.
(4) (a) Carn, F.; Colin, A.; Achard, M.-F.; Deleuze, H.; Backov, R. *Adv. Mater.* **2004**, *16*, 140. (b) Carn, F.; Colin, A.; Achard, M.-F.; Deleuze, H.; Sanchez, C.; Backov, R. *Adv. Mater.* **2005**, *17*, 62. (c) Carn, F.; Steunou, N.; Livage, J.; Colin, A.; Backov, R. *Chem. Mater.* **2005**, *17*, 644.
(5) (a) Imhof, A.; Pine, D. J. *Nature* **1997**, *389*, 948 (b) Schacht, S.; Huo, Q.; Voigt-Martin, I. G.; Stucky, G. D.; Schüth, F. *Science* **1996**, *273*, 768. (c) Carn, F.; Colin, A.; Achard, M-F.; Sellier, E.; Birot, M.; Deleuze, H.; Backov, R. J. *Mater. Chem.* **2004**, *14*, 1370. (d) Fornasieri, G.; Badaire, S.; Backov, R.; Mondain-Monval, O.; Zakri, C.; Poulin, P. *Adv. Mater.* **2004**, *16*, 1094.
(6) Jung, J. H.; Yoshiyuki, Y.; Shinkai, S. *Angew. Chem., Int. Ed.* **2000**, *39*, 1862.
(7) Hall, S. R.; Bolger, H.; Mann, S. *Chem. Commun.* **2003**, 2784.
(8) Wang, D.; Caruso, R. A.; Caruso, F. *Chem. Mater.* **2001**, *13*, 364.
(9) Livage, J. *New J. Chem.* **2001**, *25*, 1.
(10) (a) Brinker, C. J.; Scherer, G. W. In *Sol−Gel Science: the Physics and Chemistry of Sol−Gel Processing*; Academic Press: San Diego, 1990. (b) Livage, J. *Chem. Mater.* **1991**, *3*, 578.
(11) (a) Baker, L. C. W.; Glick, D. C. *Chem. Rev.* **1998**, 98, 3. (b) Hagrman, P. J.; Finn, R. C. O.; Zubieta, J. *J. Solid State Sci.* **2001**, *3*, 745.
(12) Zöcher, H. *Z. Anorg. Allg. Chem.* **1925**, *147*, 91.
(13) (a) Davidson, P.; Bourgaux, C.; Livage, J. *Adv. Mater.* **1997**, *9*, 900. (b) Livage, J.; Pelletier, O.; Davidson, P. *J. Sol−Gel Sci. Technol.* **2000**, *19*, 275.

10.1021/cm0711966 CCC: $37.00
Published on Web 07/17/2007

generating the first macroscopic fibers made of vanadium oxide with specific alcohol-sensing properties[14] while, later on, by varying the shear rate associated with the gel extrusion process, we were able to tune both the as-synthesized fibers' final mechanical and sensing properties.[15]

Fibers are in fact composites made of both poly(vinyl alcohol) (PVA) and vanadium oxide. If we demonstrated that alignment of the ribbons is playing a major role toward the fibers' final properties,[15] several issues were still unsolved, and we claimed our next work would focus on the influence of several parameters toward the fibers' properties, such as the amount of organic matter, the inorganic core crystalline character, the porosity, and again the ribbons' alignment. Beyond that, we asked ourselves if the parameters mentioned above were involved either within a cooperative or a more partitive action mode toward the fibers' sensing and mechanical properties.[15] Herein, we intend to answer the above questions where, in a first step, inclusion of latex nanoparticles within the fiber core will be proposed using two different shear rates and, second, removal of organic entities (both PVA and latex) will be induced using a thermal treatment. Finally, comparison of the fibers' sensing and mechanical performances prior to and after thermal treatment at two different shear rates will be discussed and conclusions toward the parameters action mode will be proposed.

Experimental Section

Syntheses. Dowex 50WX2-100 ion-exchange resin, sodium metavanadate (90%), and polyvinyl alcohol (hydrolyzed 87−89%) were purchased from Aldrich. Synthesis of $V_2O_5 \cdot nH_2O$ gels was performed by the ion exchange method.[9b,16−18] A solution of a sodium metavanadate ($NaVO_3$) precursor of concentration 0.1 mol/L is passed through a proton exchange resin (DOWEX-W-hydrogen, strongly acid cationic, 2% cross-linking, 50−100 mesh). While acidification occurs, the pH of the solution decreases from 7 to 2.6. At a pH close to 2, the solution starts to polymerize, and after 20 h, a dark red gel of V_2O_5 ribbons is formed. The gel vanadium weight fraction is determined by preparing a dry extract. Solutions suitable for the extrusion process have been generated by mixing appropriate amounts of vanadium oxide gel and colloidal suspension of polystyrene (latex). Latex particles (180 nm) have been obtained according to the procedure described elsewhere.[19] Weight fractions of vanadium oxide in the gel/polystyrene suspensions have been determined by dry extracts. Three different sets of solutions were prepared bearing different amounts of latex nanoparticles. Latex particles were introduced into an Erlenmeyer containing the vanadium oxide gel, and then water was added to bring the solutions to the appropriate volumes. Typically, three 50-mL solution sets were prepared containing 1.2 wt % of V_2O_5 and 0.12 wt % of latex (10 wt % of latex particle with regard to V_2O_5), 1.2 wt % of V_2O_5 and 0.36 wt % of latex (30 wt % of latex particles with regard to V_2O_5), and finally 1.2 wt % of V_2O_5 and 0.72 wt % of latex (60 wt % of latex particles with regard to V_2O_5). The as-prepared sols were left to sonicate for 10 min prior to their use for the extrusion process. These sols have to be used within a 2 day period; after that a change in color from red to green indicates some vanadium reduction. The vanadium oxide fibers were obtained by extruding the as-prepared sols into a polyvinyl alcohol (PVA) aqueous solution (1.5 wt % of PVA 1.5%). The beaker containing the PVA solution was kept at a constant rotation speed of 50 rotations per minute (rpm) while the vanadium oxide gel was extruded out of its containing syringe at a constant low flux (50 mL/h). Upon completion of the extrusion processes, the vanadium oxide threads were meticulously taken of the beaker by hand and let air-dry.

Characterization. Final inorganic fibers were then analyzed. SEM observations were performed with a JEOL JSM-840A scanning electron microscope operating at 10 kV. The specimens were carbon-coated prior examination. XRD experiments were carried out on a X'pert MPD Philips using Cu Kα (1.54 Å) radiation with an average current of 50 mA. Small-angle X-ray scattering experiemnts (SAXS) were performed with a NanoSTAR apparatus (Bruker). The X-ray source was a sealed tube X-ray generator. The Cu−Kα radiation was selected with two Göbbel mirrors and collimated with three pinholes. The scattered radiation was collected on a two-dimensional detector (HI-STAR). The diffuse scattering intensity (I) is plotted versus the scattering vector $q = (4\pi/\lambda) \sin \theta$, where 2θ is the scattering angle and λ the incident wavelength. ^{51}V MAS NMR spectra were recorded at 105.2 MHz on a Bruker Avance 400 spectrometer using a MAS 4 mm ^1H/BB probe. Vanadium oxide fibers were cut and packed in 4-mm ZrO_2 rotors. Solid samples were spun at 12.5 kHz. ^{51}V MAS NMR spectra were acquired with a rotor synchronized echo sequence ($\theta-\tau-2\theta-\tau$-acq with $\theta = \pi/16$, $\tau = 1/\nu_r$, where ν_r is the spinning frequency) and with power levels corresponding to $\pi/2$ lengths for the liquid standard (NH_4VO_3) of approximately 2.5 μs. A spectral width of 1 MHz and 0.5 s of recycle time were used. An accumulation of 43 200 transients was performed on the sample. The ESR spectra were recorded at room temperature on a Bruker Elexsys E500 spectrometer operating at X band (9.4 GHz) equipped with a SHQ cavity. A modulation of the magnetic field at 100 kHz and with amplitude = 2 G was applied to detect the absorption first derivative. The microwave power was kept at suitable low values (20 mW) to avoid saturation effects. The spin concentrations were determined by comparison of the sample ESR intensities with that of the standard DPPH (1,1-diphenyl-2-picrylhydrazyl), a sample containing 1.0066×10^{17} spins. The simulations of the ESR spectra were performed with the XSophe software (licensed by Bruker Biospin) using full matrix diagonalization. Thermogravimetric analyses (TGA) were carried out under an oxygen flux (5 $cm^3 \cdot min^{-1}$) using a heating rate of 5 °C·min^{-1}. The apparatus is a Setaram TAG-1750 thermogravimetric analyzer. Traction mechanical experiments have been performed with a ZWICKI Z2.5/TN1S apparatus at a constant traction speed of 0.3 mm/min. BET experiment have been performed using an ASAP 2010 apparatus from Micrometrics.

Results and Discussion

Fibers Preparation and Characterization at Different Length Scales. The process of synthesizing the fibers makes the use of an extrusion process where a vanadium oxide sol is expelled from a syringe needle into a rotating beaker containing a PVA solution (Figure 1a). As-synthesized fibers can be taken off the beaker vertically and suspended above the beaker in order to drain the excess of PVA solution. After drying it is possible to generate fibers possessing several

(14) Biette, L.; Carn, F.; Maugey, M.; Achard, M.-F.; Maquet, J.; Steunou, N.; Livage, J.; Serier, H.; Backov, R. *Adv. Mater.* **2005**, *17*, 2970.
(15) Serier, H.; Achard, M.-F.; Steunou, N.; Maquet, J.; Livage, J.; Leroy, C.; Babot, O.; Backov, R. *Adv. Funct. Mater.* **2006**, *16*, 1745.
(16) Pelletier, O.; Davidson, P.; Bourgaux, C.; Coulon, C.; Regnault, S.; Livage, J. *Langmuir* **2000**, *16*, 5295.
(17) Vigolo, B.; Zakri, C.; Nallet, F.; Livage, J.; Coulon, C. *Langmuir* **2002**, *18*, 9121.
(18) Lemerle, J.; Nejem, L.; Lefebvre, J. *J. Inorg. Nucl. Chem.* **1980**, *42*, 77.
(19) Imhof, A. *Langmuir* **2001**, *17*, 3579.

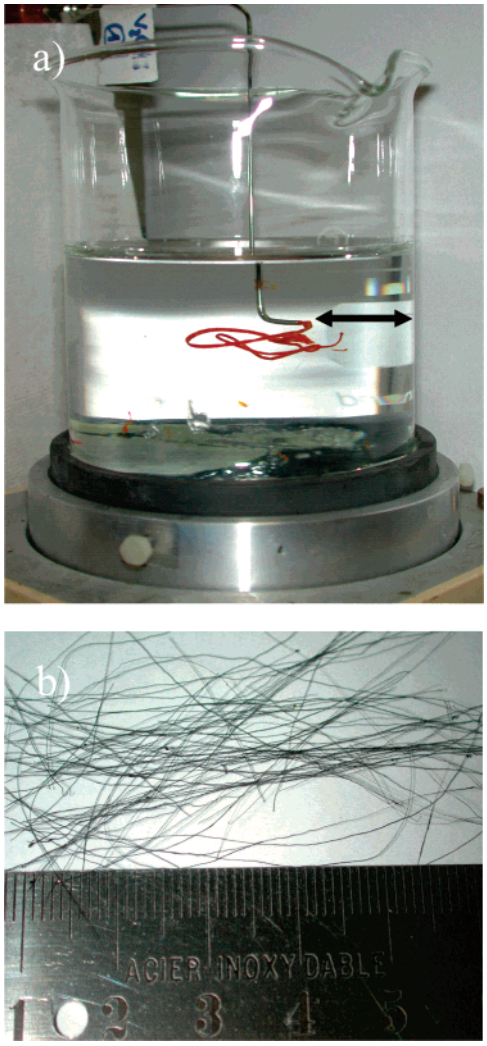

Figure 1. (a) Experimental setup allowing the fiber extrusion (The black double arrow indicates the distance of the needle head from the outer part of the beaker) and (b) several dried fibers.

centimeters of length (Figure 1b). When comparing parts a and b of Figure 1, we can observe that the fibers undergo substatial shrinkage when drying.

As explained and expressed elsewhere[15] the distance of the needle head from the external part of the rotating beaker is directly related to the imposed shear rate on the extruded sol (Figure 1a, black arrow). Note that there is no shear stress applied to the sol within the syringe, since the hydrophilic sol does not wet the internal stainless steel surface, which is rather hydrophobic (the flux within the syringe is not a "Poiseuil" type but rather a "plug" one). Thus the shear stress is only addressed when the outflowing sol is in contact with the PVA rotating solution. The shear rate $\dot{\gamma}$ respectively equals 235 and -158 s^{-1}), and the latex concentrations (10, 30, and 60 wt %) have been systematically varied. When the sol is extruded, the wet fibers are then extracted from the rotating beaker and suspended to drain the excess of PVA solution and let air-dry. These as-synthesized fibers are then submitted to a thermal treatment at 350 °C in air to promote porous inorganic fibers from the vanadium oxide/latex/PVA composites. Mechanical and sensing properties were tested prior to and after applying the thermal treatment. Figure 2 shows the effect of thermal treatment on the fibers' textures

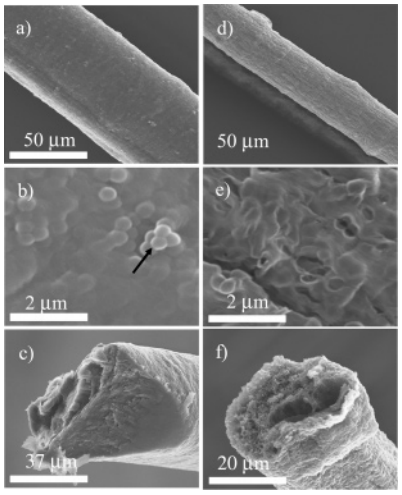

Figure 2. SEM pictures of fibers obtained with a 60 wt % latex concentration and under a shear rate of -158 s^{-1}. (a−c) Without thermal treatment and (e, f) after thermal treatment at 350 °C. The black arrow indicates an aggregate of the latex nanoparticles.

Table 1. Carbon and Vanadium Percentage Evaluated from EDX Semiquantitative Experiments

composite V_2O_5/PVA/latex fibers				thermally treated V_2O_5 fibers			
latex (%)	shear rate (s^{-1})	wt % V	wt % C	from latex (%)	shear rate (s^{-1})	wt % V	wt % C
10	−158	49	51	10	−158	96	4
10	235	36	64	10	235	87	4
30	−158	31	70	30	−158	93	5
60	−158	28	72	60	−158	90	7
60	235	17	83	60	235	96	4

at the macroscopic length scale via scanning electron microscopy (SEM).

As shown with Figure 2 the thermal treatment at 350 °C is accompanied with a strong shrinkage of the fibers, associated with native void spaces (images e and f of Figure 2) that replace the latex nanoparticles in use (Figure 2b, black arrow). Also we can notice that the latex nanoparticles remain randomly aggregated, despite the sonication of the starting sols. An overall shrinkage effect of around 50% (comparing, for instance, parts a and d of Figure 2) is observed after the thermal treatment. Beyond this contemplative experiment, we performed at the same time some energy dispersive X-ray analyses (EDX) as semiquantitative experiments to estimate the carbon/vanadium ratios (Table 1), revealing that the calcined fibers still possess some residual carbon (around 5%).

At the mesoscopic length scale, we can notice that an increase of latex concentration, affects the preferential organization of the nanoribbons' subunits inside the fibers, as observed with cross-polarized optical microscopy and small-angle X-ray scattering (SAXS) experiments (Figure 3).

We already demonstrated that the ribbons' subunits are preserved within the as-synthesized fibers,[13,14] and as direct evidence of the high-scale organization of the ribbons' subunits, the macroscopic fibers depict maximum birefringence when positioned at 45° between the analyzer and polarizer of the optical microscope in use (Figure 3a−c). We can notice a decrease of the brightness both as the latex concentration is increased while the shear rate is maintained

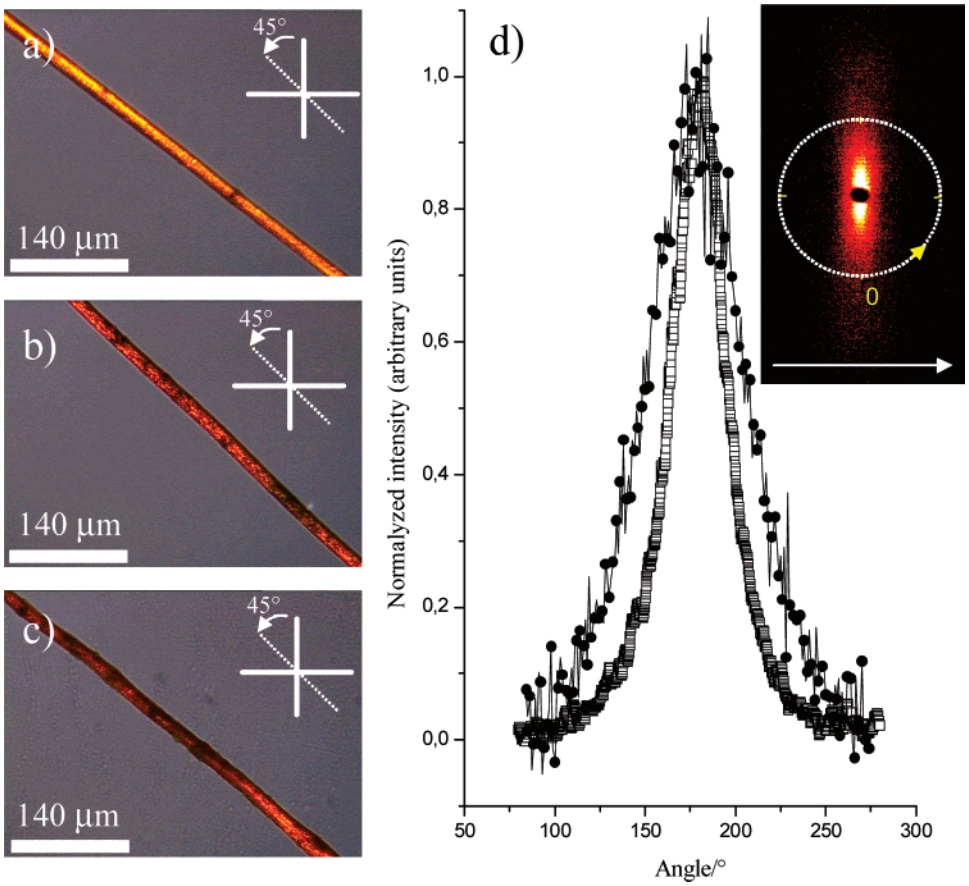

Figure 3. (a−c) Fibers observed through cross-polarized optical microscopy, (a) 10 wt % latex and $\dot{\gamma} = 235\ s^{-1}$, (b) 10 wt % latex and $\dot{\gamma} = -158\ s^{-1}$, (c) 60 wt % latex and $\dot{\gamma} = 235\ s^{-1}$. (d) SAXS spectra: □, 0 wt % latex and $\dot{\gamma} = 235\ s^{-1}$; ●, 60 wt % latex and $\dot{\gamma} = 235\ s^{-1}$. (The embedded figure depicts the anisotropic diffuse pot with the fiber main axis being postioned parallel to the white arrow).

constant (Figure 3a,c) and as the applied shear rate is decreased while the latex amount is maintained constant (Figure 3a,b). Nevertheless, this observation is not sufficient to assess that the ribbons preferential orientation is disturbed by latex adjunction, since the polymeric nanoparticles also diminish the light transmission during the optical microscopy experiments (transmission mode used for the cross-polarized optical experiments). We thus make the use of SAXS experiments to better qualify the effect (Figure 3d). As previously reported,[14] an anisotropic X-ray pattern is observed in the small angles region, revealing a preferred orientation of the V_2O_5 ribbons along the fibber axis. The analysis of the angular intensity profile allows appreciating the degree of alignment of the ribbons within the fiber. As shown in Figure 3d, the angular distribution of the ribbons (evaluated as the width at half-height of the angular intensity profile) is clearly wider for latex-containing fibers than for pure V_2O_5 fibers. This observation suggests that the latex particles disturb the alignment of the vanadium oxide nanoribbons inside the fibers. Also at the mesocopic length scale we performed some nitrogen adorption−desorption measurements on fibers before and after thermal treatment. The overall porosity addressed with the BET method were very low, around 17 $m^2\ g^{-1}$, without any evolution as the latex content increases, going from 10 to 60 wt %. This feature is normal, considering the size of the latex particles (180 nm) and the BET application limits over the pore sizes characterization (10 Å to 10 nm at best). On the other hand,

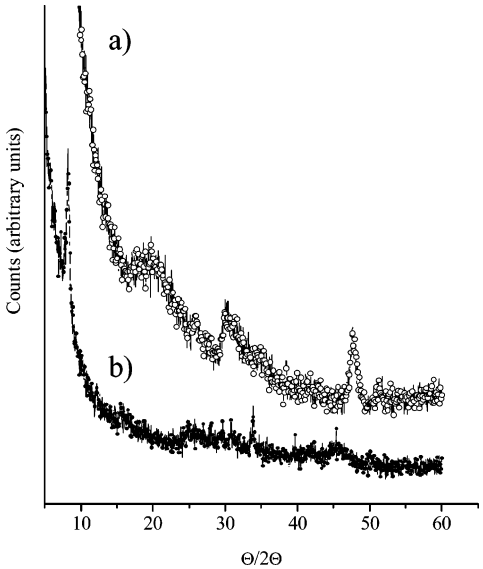

Figure 4. XRD patterns (a) composite fibers and (b) calcined fibers.

this experiment demonstrates that the nanoribbons are strongly packed, avoiding any inter-ribbon mesoporosity.

Microscopically, the X-ray diffraction pattern (XRD) (Figure 4a) of the uncalcined fibers depicts a quasiamorphous character, as already observed for similar fibers obtained without inclusion of latex particles.[14] After thermal treatment at 350 °C in air, we can see (Figure 4b) that there is a weak increase of the sample's crystalline character, and the major diffraction patterns associated with the PVA polymeric chains

(20°/2Θ) are vanished while the 00l Bragg diffraction intensity associated with the vanadium oxide interlayer gallery distance is enhanced. The two diffraction patterns were taken using fibers powdered using a mortar; thus, the above feature is not a preferential orientation phenomenon.

At the temperature applied during the thermal treatment, the vanadium oxide is not yet completely crystallized; thus, we had to specify the vanadium local environment with certainties. In this issue, XRD investigation is by far not enough by itself. We then first performed some V^{51} NMR where the V_2O_5/PVA/60 wt % latex fibers were characterized by ^{51}V MAS NMR spectroscopy. The ^{51}V MAS NMR spectrum displays a very broad signal covering almost 1000 ppm (not shown here). This poor resolution is certainly due to a large concentration of paramagnetic V^{4+} centers. A disorder in the material may also contribute to this line broadening. Indeed, as discussed above, the introduction of latex particles in the composite material disturbs the alignment of the V_2O_5 ribbons, as shown by SAXS measurements when compared to the pure V_2O_5 fibers.[14,15] Therefore, these fibers were also investigated by ESR spectroscopy. In order to compare the local environment of V^{4+} ions in the calcined fibers with pure V_2O_5 fibers, we report the ESR spectrum of pure V_2O_5 fibers (Supporting Information Figure 1). A single ESR line with peak-to-peak line width $\Delta B_{pp} \approx 95$ G is observed at $g = 1.9701(9)$ for the pure V_2O_5 fibers, as previously reported.[14] The value of the g factor is consistent with V^{4+} species. The hyperfine splitting due to the interaction with the ^{51}V nucleus ($I = 7/2$, 99.8% natural abundance) and the g factor anisotropy are not observed in this spectrum. The reason is the occurrence of a narrowing phenomenon probably due to spin−spin exchange interactions between V^{4+} species, but an electron hopping process between V^{4+} and V^{5+} centers cannot be ruled out. In contrast, the ESR spectrum of the calcined fibers (Figure 5) is different, suggesting a redistribution of V^{4+} centers in the material. This spectrum is made of several overlapping signals.

First, one can notice a single line indicated by a star in Figure 5a at $g = 2.0018(9)$ and with a peak-to-peak line width $\Delta B_{pp} \approx 8$ G. This signal is very similar to those usually observed in carbonaceous materials[20] and thus most probably arises from carbonaceous radicals, highly depleted in heteroelements, produced by the calcination of the organic components in the fibers, in agreement with results emerging from EDS (Table 1). The ESR spectrum also contains two broad structureless signals (Figure 5b), the first one at $g \approx 2.13$ and with $\Delta B_{pp} \approx 1000$ G, probably due to transition metal impurities, and the second one at $g \approx 1.963$ and with peak-to-peak line width $\Delta B_{pp} \approx 181$ G. This latter signal can be attributed to spatially close V^{4+} species in exchange interaction or to an electron hopping process. Similar EPR spectra were previously reported for $V_2O_5{\cdot}nH_2O$ gels with a V^{4+}/V_T ($V_T = V^{5+} + V^{4+}$) ratio ranging from 3 to 15%.[10b,21] The exchange (or electron hopping) mechanism

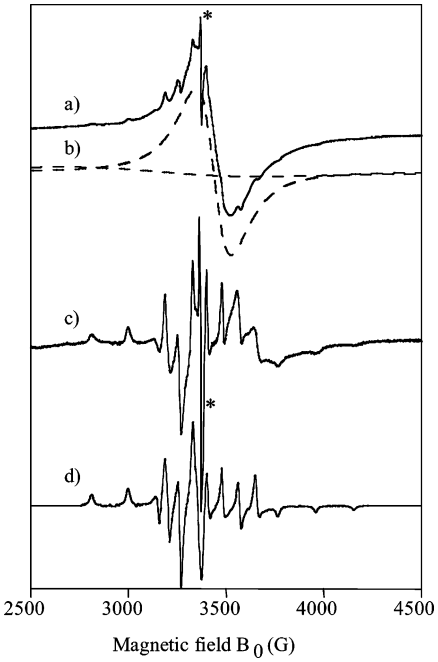

Figure 5. ESR spectrum of the calcined V_2O_5/PVA/60 wt % latex fibers recorded at room temperature. (a) Experimental spectrum. The star indicates the ESR line of carbonaceous radicals at $g = 2.0018$. (b) Calculated background Lorentzian lines with $g = 1.963$, peak-to-peak line width = 181 G and $g = 2.13$ and peak-to-peak line width = 1000 G. (c) Spectrum of VO^{2+} obtained by substraction of the background lines (b) from spectrum (a). (d) Calculated spectrum with parameters $g_{||} = 1.936$, $g_{\perp} = 1.976$, $A_{||} = 192$ G, and $A_{\perp} = 71$ G.

may be due to either a large amount of V^{4+} ions in the material or a local concentration of V^{4+} centers that are not evenly distributed through the gel. Assuming the relative integrated areas of both spectra, it appears that the amount of V^{4+} species is twice than that of in the pure V_2O_5 fibers. This may explains the poor resolution of the ^{51}V MAS NMR spectrum. This reduction of V^{5+} entities may occur upon addition of latex particles to the V_2O_5 sol, since the solution turned green or may be due to the combustion of organic groups upon heating. A similar reduction process was previously proposed for the hydrothermal synthesis of mixed valence vanadium oxides.[22] When the two broad signals of Figure 5b are substracted from the ESR spectrum of Figure 5a, a fourth signal is revealed (Figure 5c) typical of isolated vanadyl VO^{2+} ions in an axial crystal field and with a well-resolved hyperfine structure due to the interaction between the unpaired electron spin on V^{4+} and the ^{51}V nuclear spin. Figure 5d shows the simulated spectrum with the following spin Hamiltonian parameters: $g_{||} = 1.936(1)$, $g_{\perp} = 1.976(1)$, $A_{||} = 192(2)$ G, and $A_{\perp} = 71(2)$ G. These parmeters are also listed in Table 2 along with the ESR parameters from the literature for related materials, such as amorphous V_2O_5 (hydrated and dehydrated), $V_2O_5{\cdot}nH_2O$ gels (hydrated and dehydrated), crystalline V_2O_5, and $[VO(H_2O_5)_5]^{2+}$. The EPR parameters for the calcined fibers are in fair agreement with those of $V_2O_5{\cdot}nH_2O$ gels (see Table 2). In particular, the $g_{||}$ value is close to that of a hydrated V_2O_5 gel. Actually, it was previously reported that hydration of V_2O_5 gels is generally associated with an increase of the $g_{||}$ (and to a lesser

(20) Retcofsky, H. L.; Stark, J. M.; Friedel, R. A. *Anal. Chem.* **1968**, *40*, 1699.

(21) (a) Wiench, J. W.; Fontenot, C. J.; Woodworth, J. F.; Schrader, G. L.; Pruski, M.; Larsen, S. C. *J. Phys. Chem. B* **2005**, *109*, 1756. (b) Babonneau, F.; Barboux, P.; Josien, F. A.; Livage, J. *J. Chim. Phys.* **1985**, *82*, 761.

(22) Bouhedja, L.; Steunou, N.; Maquet, J.; Livage, J. *J. Solid State Chem.* **2001**, *162*, 315.

Table 2. EPR Parameters for Vanadium Oxide Compounds

	$g_{\|\|}$	$g_\perp$	$A_{\|\|}(G)$	$A_\perp(G)$	ref
$V_2O_5 \cdot 0.5H_2O$[a]	1.925	1.982	196	76	10b
$V_2O_5 \cdot 1.8H_2O$[a]	1.935	1.986	204	78	10b
amorphous V_2O_5					
dehydrated	1.913	1.98	176	66	23
hydrated	1.932	1.977	198	74.5	23
V_2O_5 gel					
dehydrated[b]	1.915	1.970	193	74.3	21a
hydrated[b]	1.930	1.990	195	74.5	21a
crystalline V_2O_5	1.923	1.986	190	73	10b
$[VO(H_2O)_5]^{2+}$	1.934	1.987	203	66	10b
calcined V_2O_5/PVA/latex 60% fibers	1.936(1)	1.976(1)	192(2)	71(2)	this work

[a] Gel prepared by acidification of $NaVO_3$ with a proton exchange resin. [b] Gel prepared by dissolution of crystalline V_2O_5 with H_2O_2.

extent the $A_{\|}$ value).[10b,21a,23] It suggests that the crystal fields arount V^{4+} ions in V_2O_5/PVA/60 wt % latex fibers are similar to that of $[VO(H_2O)_5]^{2+}$, which is a strongly distorted VO_6 octahedron with a short V−O bond along the *z*-axis and a long V−OH_2 bond in the trans position.

Fibers Mechanical Properties: Effect of the Latex Particles Content, Applied Shear Rates, and Thermal Treatment. The fibers' mechanical properties depend not only on the specific alignment of the nanoscopic ribbon subunits as previously demonstrated[15] but also strongly depend on the amount of organic matter that composed the fibers. To assess longitudinal mechanical properties, several traction measurements have been performed over each set of fibers (Figure 6).

Figure 6a presents the evolution of the fibers' mechanical behavior at a constant shear rate of $-158\ s^{-1}$ versus the latex contents. An increase of the plastic regime is observed as the amount of the latex increases. This effect is expected for the following two main reasons: first, as the latex amount is increasing from 10 wt % to 60 wt %, the fibers overall mechanical behavior will be more and more directed by the latex intrinsic mechanical nature, i.e., a plastic behavior; second, as we increase the latex amount, we increase the perturbation addressed over the ribbons' subunits alignments during the shear rate (Figure 3d). In addition, we have previously demonstrated that a decrease of the ribbons' preferential alignment toward the fiber main axis results with an increase of the plastic regime obtained when performing traction experiments.[15] As a direct consequence, the Young's modulus (E) is decreasing as the latex amount increases (Table 3). The same tendency is observed for the rigidity (σ). The Figure 6b underlines the effect of the applied shear rates. For the latex contents 10 and 60 wt % we can see that the effect of the applied shear rate is roughly the same, namely we observe a decrease of the plastic regime (weak decrease for the 10%) associated with a decrease of the Young modulus and plasticity as the shear rate increases from -158 to $235\ s^{-1}$ (Table 3). Despite an overall similarity when considering the effect of the shear with the latex contents of 10 and 60 wt %, we can observe that the Young's modulus variation with the applied shear rate is weak for the fibers containing 60 wt % (10 and 11 GPa, respectively, for shear rates of 235 and $-158\ s^{-1}$), while the Young's modulus for the fibers with a latex of 10 wt % varies much more from 22 to 16 GPa when respectively applying shear rates of 235 and $-158\ s^{-1}$ (Table 3).

In fact, this feature demonstrates that the latex particles are perturbing the nanoribbons' alignments, specially for high latex contents. As is the case for the fibers containing 60 wt % latex, the particles' isotropic character is smoothing the shear rate effect, and as a direct consequence, the obtained Young's modulus values, when varying the shear rates from 235 to $-158\ s^{-1}$, are almost the same (Table 3). Figure 6c,d depicts the fibers mechanical properties once the thermal treatment has been applied. Overall, we can see that there is a severe decrease of the fibers mechanical properties, whatever the shear rate applied and the starting latex contents. In Figure 6c we can observe that fibers generated from the higher latex content (60 wt %) and the lower shear rate ($-158\ s^{-1}$) depict the weaker mechanical properties associated with a weak Young's modulus of 0.5 GPa (Table 3); again, this feature is quite expected, as void spaces induced by the thermal treatment are replacing the latex nanoparticles. In Figure 6d we can notice that the effect of the applied shear rate over the calcined fibers is weak, whatever the starting latex contents.

Fibers' Sensing Properties: Effect of the Latex Particles Content, Shear Rates, and Thermal Treatment. As mentioned before,[14,15] the intrinsic one-dimensional nature of the as-synthesized vanadium oxide fibers allows generating sensing cells with a certain degree of simplicity. We previously demonstrated that PVA/vanadium oxide fibers were able to sense 0.1 ppm of ethanol within 16 s at 40 °C, with good cycling properties and selectivity toward diverse alcohols.[14,15] The goal of this study is first to search for higher sensitivity and good cycling properties associated with enhanced thermodynamic stability. Beyond this, the sensing results will be discussed in terms of the nanoribbons' alignments, the latex contents, and the effect of the removal of the latex. Results considering the fiber sensibilities are provided for uncalcined and calcined fibers within Figures 7 and 8, respectively.

In Figure 7a we can notice that the effect of latex concentration over the sensing properties is rather weak, with a soft trend that intends to show that an increase of the latex content allows optimizing the sensing properties. For instance, at 42 °C the sensing time to detect 0.1 ppm of ethanol decreases from 11 to 9 s when increasing the latex contents respectively from 10 to 60 wt %. At first glance, we are in the limit of the error (1.5 s) for the time detection, and considering this issue, we would say that the effect of the latex contents, at a constant shear rate, cannot be detected with the apparatus in use but stays overall within the same range when compared with vanadium oxide fibers free of latex particles.[14,15] Figure 7b shows the effect of both latex content and shear rate applied during the extrusion process. Here again, we can notice that the effects are very weak with a soft tendency to increase the sensing properties as the applied shear rate increases, a fact that is expected, as increasing the shear rate allows a better alignment of the nanoribbons, subunits,[15] a feature that eases the generation

(23) Nabavi, M.; Sanchez, C.; Livage, J. *J. Philos. Mag. B* **1991**, *63*, 941.

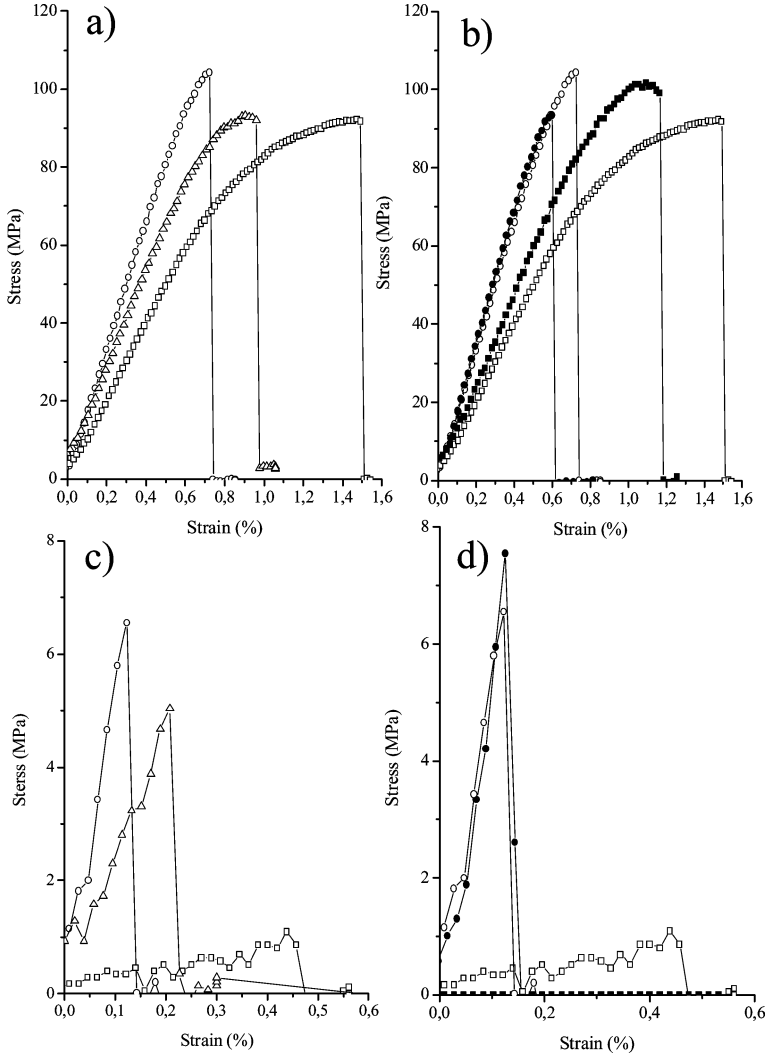

Figure 6. Fiber mechanical properties versus the imposed shearing rates and the latex content. Measurements were performed at a strain rate of 0.3 mm/min. (a) latex content at a constant shear rate $\dot{\gamma}$ equal to -158 s^{-1}: ○, 10 wt % latex; △, 30 wt % latex; □, 60 wt %. (b) Effect of shear rates and latex contents: ○, 10 wt % latex and $\dot{\gamma}$ equal to -158 s^{-1}; ●, 10 wt % latex and $\dot{\gamma}$ equal to 235 s^{-1}; □, 60 wt % latex and $\dot{\gamma}$ equal to -158 s^{-1}; ■, 60 wt % latex and $\dot{\gamma}$ equal to 235 s^{-1}. (c and d) Same conditions for the calcined fibers.

Table 3. Mechanical Characteristics for the Vanadium Oxide Fibers at Each Applied Shearing Rates and Organic Contents[a]

Composite V_2O_5/PVA/Latex fibers						
latex (%)	shear rate (s^{-1})	E (Gpa)	σ_{max} (MPa)	ϵ_{max} (%)	$\sigma_{breaking}$ (MPa)	$\epsilon_{breaking}$ (%)
10	−158	15.9	107.1	0.8	107	0.8
10	235	22.0	109.5	0.6	103	0.7
30	−158	14.0	102.1	0.9	98	1.0
60	−158	11.2	101.6	1.4	100	1.5
60	235	10.3	98.3	1.2	95	1.3
Thermally Treated V_2O_5 Fibers						
from latex (%)	shear rate (s^{-1})	E (Gpa)	σ_{max} (MPa)	ϵ_{max} (%)	$\sigma_{breaking}$ (MPa)	$\epsilon_{breaking}$ (%)
10	−158	5.4	7.6	0.2	7.7	0.2
10	235	4.0	5	0.2	5	0.2
30	−158	1.8	6.7	0.3	6.7	0.3
60	−158	0.5	1.5	0.4	1.5	0.4
60	235	0	0	0	0	0

[a] Measurements were performed at a strain rate of 0.3 mm/min. E is the Young's modulus, σ and ϵ respectively represent the stress and strain before breaking.

of conductor domains taking into account the following scenario. The conductivity mechanism associated with the alcohol-sensing effect has been hypothesized elsewhere in terms of surface charge electron-depletion strongly associated with the O−H bonds ionic character.[24] Under a source of alcohol vapors, the alcohol can be adsorbed onto vanadium oxide ribbons by hydrogen bonds. Second, due to the ionic character of the OH group and its associated acidity, anionic charges are created at the outer ribbons' subunits surface that promotes a statistical electron release, i.e., conductive domains that grow to finally form the depletion layer (Scheme 1). Considering that the nanoribbons are statistically connected together, via hydrogen bonds within the macroscopic fibers, then electrons can pass through the entire fiber, which becomes an electronic conductor. The better the alignment of the nanoribbon subunits, the higher the sensitivity generated. Comparing Figures 7 and 8 it is obvious that the fibers sensitivity is increased when removing most of the organic content of the fibers. In fact, both PVA and latex are insulator components, and their removal will thus enhance the fiber's intrinsic conductivity. The detection time, for calcined fibers, has been overall divided by three; specifically

(24) (a) Micocci, G.; Serra, A.; Tepore, A.; Capone, S.; Rella, R.; Siciliano, P. J. *Vac. Sci. Technol., A* **1997**, 15, 34. (b) Liu, J.; Wang, X.; Peng, Q.; Li, Y. *Adv. Mater.* **2005**, *17*, 764.

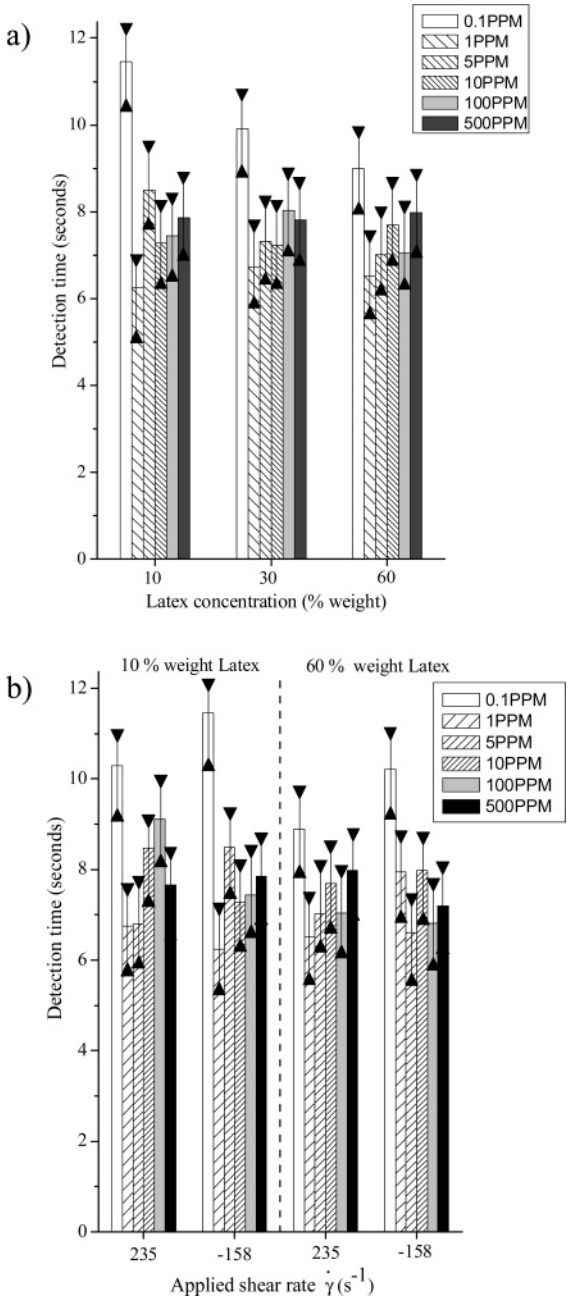

Figure 7. Histograms that depict ethanol sensitivities at 42 °C for uncalcined vanadium oxide fibers. The experimental setup has a fiber placed above a beaker containing ethanol for which the concentration varies from 500 ppm down to 0.1 ppm. Ethanol has been diluted into THF because THF does not promote any effect over the conductivity cell. The provided results have been obtained for a single vanadium oxide fiber. (a) Effect of latex contents at constant shear rate of 235 s^{-1} and (b) effects of both latex contents and applied shear rate.

0.1 ppm of ethanol at 42 °C can be now detected within 3−5 s (Figure 8).

Again, the effect of porosity, emerging from the removal of the starting latex and PVA contents (Figure 8a), and the effect of the applied shear rate (Figure 8b) over the detection time are very hard to analyze, as again the difference observed are basically within the limit (1.5 s) of the time detection error. Basically, we can state that the effect of porosity and applied shear rate do not perturb much the sensing properties of these final vanadium oxide fibers, while the overall sensitivity is enhanced due to the removal of PVA, which is an insulator component.

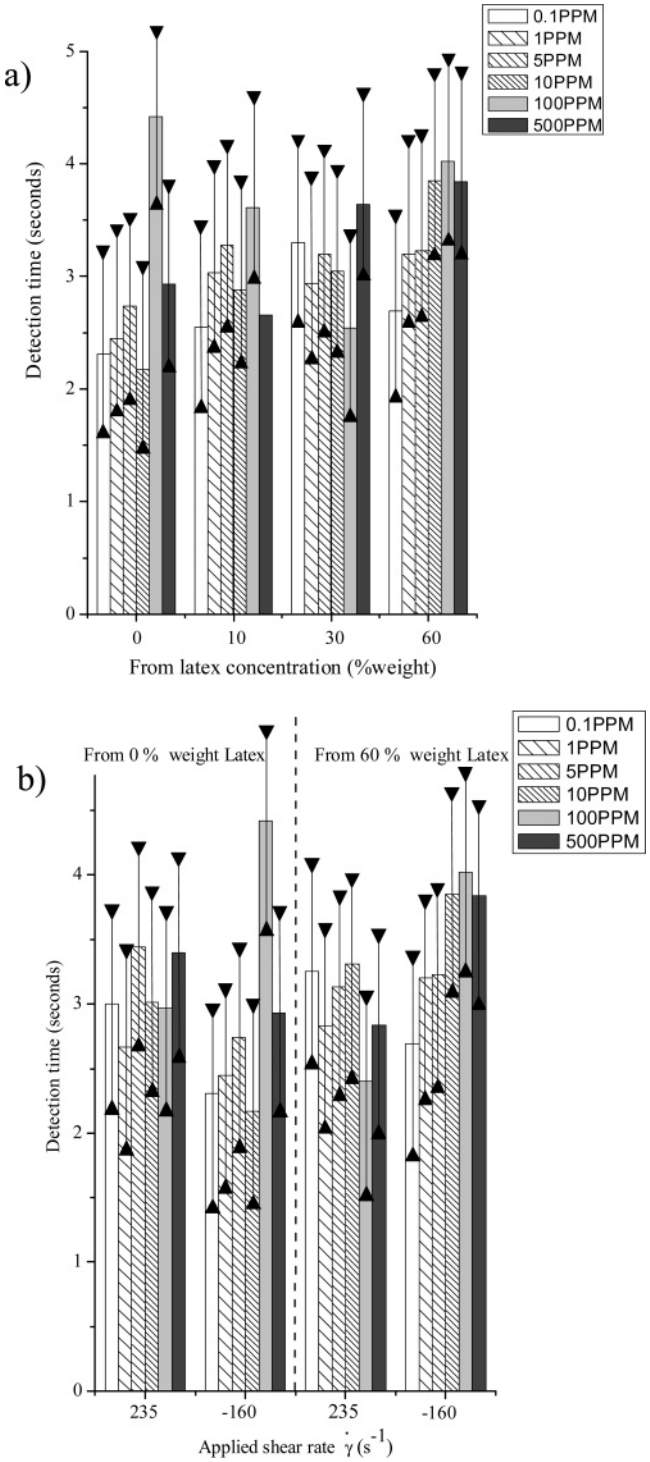

Figure 8. Histograms depicting the ethanol sensitivities at 42 °C for calcined fibers. The experimental setup has a fiber placed above a beaker containing ethanol for which the concentration varies from 500 ppm down to 0.1 ppm. Ethanol has been diluted into THF because THF does not promote any effect over the conductivity cell. The provided results have been obtained for a single vanadium oxide fiber. (a) Effect of latex contents at 235 s^{-1} and (b) effects of latex contents and applied shear rate.

Beyond kinetic characteristics, it is important to provide the thermodynamic stabilities of the as-synthesized fibers. For this issue, we let each fiber, obtained at different shear rates and latex contents (and their removal by thermal treatment), to rest above pure ethanol vapor and we then observed the conductivity evolution versus time exposure. Results are provided within Figure 9. Considering the

Scheme 1. Scenario That Depicts the Surface Electronic Depletion Mechanism (scheme mainly extracted from ref 24b)

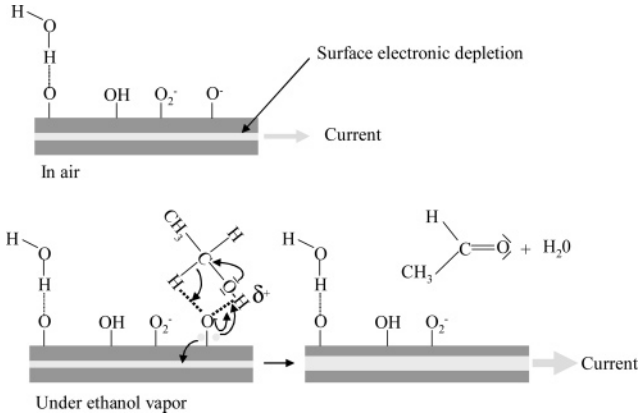

uncalcined fibers (Figure 9a,b), in a first step we can notice that for each set of fibers the conductivity is increasing as a function of the time exposed; then within a second step the conductivities increase slowly to a maximal value (or a pseudoplateau), corresponding to the thermodynamic equilibrium. First, considering Figure 9a, we can notice that the maximal value of conductivity is directly related with the latex content. This feature is normal, as the latex particles are mainly insulator in nature and the maximum of conductivity, at the thermodynamic equilibrium, will decrease as the amount of latex is increasing from 10 to 60 wt %. Considering Figure 9b, which combines the effect of the shear rates applied and latex contents, we can observe that an increase of both the latex concentrations and the shear rate applied is increasing the maximum value of conductivity at the thermodynamic equilibrium. Again, this behavior is expected and observed elsewhere for fibers without latex particles,[15] where the maximal values of conductivity were directly related with the applied shearing rate, i.e., the higher alignment of the nanoscopic ribbons' subunits constituting the macroscopic fibers is offering the higher conductivity at the thermodynamic equilibrium. This fact demonstrates that the nanoribbons' alignment is of crucial importance for the observed conductivity. In the present case, the effect of the applied shear rates over the maximum conductivity reached at thermodynamic equilibrium is much more important for the latex content of 60 wt % than 10 wt %. As the latex content is perturbing the nanoribbons' subunits alignments (Figure 3), the effect of the applied shear rate will circumventer the initial perturbation induced by the latex content. Considering Figure 9a,b, we can notice that in both cases the pseudoplateau attributed to the thermodynamic equilibrium is followed by a decrease of conductivity. The decrease of conductivity is almost the same for fibers generated at shear rates of 235 and $-158\ s^{-1}$, but it is lower for the higher amount of latex contents, 60 wt %. Whatever the shear rate employed, fibers are finally changing their color from red to green, meaning that part of the vanadium 5+ is reduced into vanadium 4+, and in the mean time they become more fragile mechanically. In the present case, increasing the latex content will promote higher perturbations over the ribbons' alignment, thus enhancing defects within the fibers core. For the fibers obtained with a maximum of latex content, while the major part of the vanadium 5+ present at the fiber outer part is reduced to vanadium 4+ (acting as a hole potential for the electrons), the ethanol might diffuse deeper into the fiber core, creating thus a subdepletion layer that, in terms of conductivity, compensates for the decreasing conductivity of the first one. This process can act until the complete part of the vanadium 5+ of the full fiber core has been reduced and the whole fiber is damaged. For the smaller amounts of latex, the applied shear rate will now be able to control the ribbons' alignments, promoting a higher packing density of the nanoribbons' subunits, thus avoiding any alcohol diffusion into the fiber core; at that point, when the outer vanadium 5+ is reduced into vanadium 4+ and the associated layer is damaged, the surface conductivity is decreasing without any compensation. We observed this issue elsewhere playing only with the applied shear rate.[15] We intended to play with the amount of latex and its removal to validate the above scenario; if the scenario is valid, then enhanced porosity will increase the alcohol diffusion phenomenon, thus enhancing the fibers thermodynamic stability. Considering Figure 9c,d, this is exactly what we observe. First, the conductivity values at thermodynamic equilibrium are higher than the ones obtained prior the calcination treatments; this effect is induced both because of the insulator (PVA and latex) counterpart removal and the small enhanced crystallization. More importantly, we can see now that the fibers are much more stable under alcoholic vapor (Figure 9c,d); particularly, the stability increases as the induced porosity increases, the fibers that depict the higher stability being the ones emerging from the 60 wt % latex contents. Considering Figure 9d, we find here the same trend concerning the effect of the shear rate over the thermodynamic stability as the one observed for fibers free of latex particles: [15] when the shear rate increases the fibers stability decreases. As a direct consequence, the fibers promoted through the lower shear rate and from the higher latex content are associated with the higher stability, because we just optimize the alcohol diffusion within the fibers' core and thus the number of electronic pathways of the sublayers that allow maintaining the conductivity at a maximal value. This particular study renders valid the scenario where sublayers can relay the conductivity process when the upper layer V^{5+} sites are reduced. Beyond thermodynamic stability, we have checked if the as-synthesized fibers are cycling when subjected to alcohol vapor or not; the results are proposed within Figure 10. Considering Figure 10, we can see that the fibers are cycling. This feature is expected, as it was already observed with the first vanadium oxide generated using the extrusion process mentioned herein.[14] The general trend is strongly related to that observed above when discussing thermodynamic stability and surface electron depletion, which explain the obtained sensitivities. First, considering Figure 10a,b we can observe that the uncalcined fibers are cycling nicely, and the maximum conductivity values are obtained for the lower amount of latex contents (Figure 10a) and the higher applied shear rate (Figure 10b). Also, considering Figure 10b, we can notice a certain decrease of the maximal conductivity values as the cycling

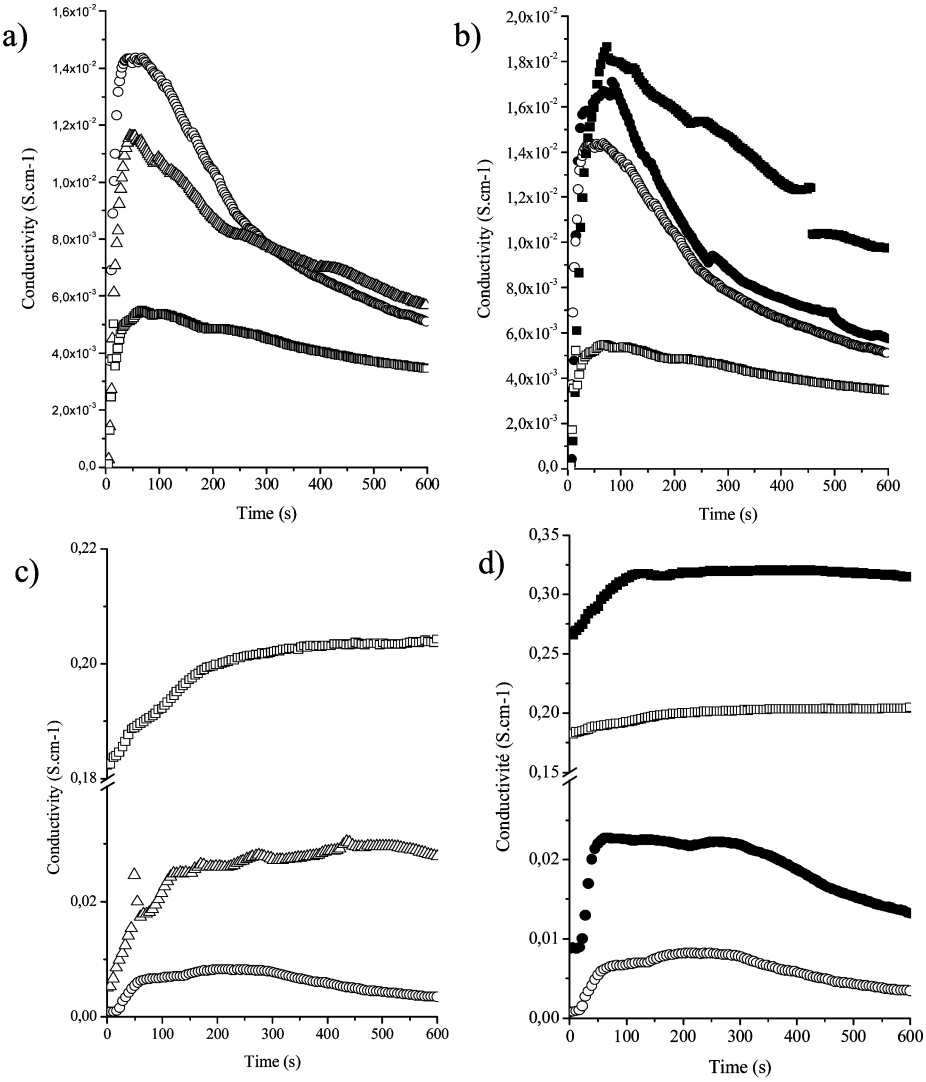

Figure 9. Evolution with time of the vanadium oxide fibers conductivity profiles at 42 °C when placed above a beaker containing pure ethanol. The results have been obtained for a single vanadium oxide fiber. (a) Latex contents at a constant shear rate $\dot{\gamma}$ equal to -158 s^{-1}: ○, 10 wt % latex; △, 30 wt % latex; □, 60 wt %. (b) Effect of shear rates and latex contents: ○, 10 wt % latex and $\dot{\gamma}$ equal to -158 s^{-1}; ●, 10 wt % latex and $\dot{\gamma}$ equal to 235 s^{-1}; □, 60 wt % latex and $\dot{\gamma}$ equal to -158 s^{-1}; ■, 60 wt % latex and $\dot{\gamma}$ equal 235 s^{-1}. (c) Effect of latex contents over calcined fibers at a constant shear rate $\dot{\gamma}$ equal to -158 s^{-1}: ○, 10 wt % latex, △, 30 wt % latex, □, 60 wt %. (d) Effect of shear rates and latex contents over calcined fibers: ○, 10 wt % latex and $\dot{\gamma}$ equal to -158 s^{-1}; ●, 10 wt % latex and $\dot{\gamma}$ equal to 235 s^{-1}; □, 60 wt % latex and $\dot{\gamma}$ equal to -158 s^{-1}; ■, 60 wt % latex and $\dot{\gamma}$ equal to 235 s^{-1}.

runs go on, a phenomenon especially true for fibers obtained under the higher shear rate (235 s^{-1}), a feature that is not true anymore when the applied shear rate is lowered down to -158 s^{-1}. This phenomenon is in direct relationship with the above study concerning the thermodynamic stability, i.e., the fibers' stability increases as the shear rate applied is diminished. Considering the calcined fibers (Figure 10c,d), we can first observe that the fibers' cycling capabilities are strongly minimized as the starting latex content increases (Figure 9c) and that this effect can be cancelled by increasing the applied shear rate from -158 to 235 s^{-1} (Figure 10d). In fact, the thermodynamic stability and the enhanced porosity reached upon increasing the starting latex contents from 10 to 60 wt % appears as strong penalties toward the alcohol vapor desorption kinetic process. As observed in Figure 10d, considering the calcined fibers obtained through the higher latex content and the lower shear rate, the cycling curves are very smooth, and as the cycling runs go on we can barely distinguish the conductivity related with the ethanol adsorption or desorption processes.

Conclusions

Both composite vanadium oxide/PVA/latex and inorganic vanadium oxide macroscopic fibers have been generated by using an extrusion process. Specifically, inorganic vanadium oxide fibers enable the detection of 0.1 ppm of ethanol within 3−5 s at 42 °C, which is certainly one of the highest sensitivities to date concerning alcohol sensors. More importantly, by varying the starting latex inclusion contents, the shear rates associated with the gel extrusion process, and thermal treatment we were able to segregate each parameter involved within the mechanical and sensing properties associated with these as-synthesized fibers, i.e., the organic counterpart amount, the degree of vanadium oxide ribbons' alignment, and the induced porosity reached upon latex removal. The effect of the applied shear rate, despite the perturbation induced by the latex particles inclusion, is still

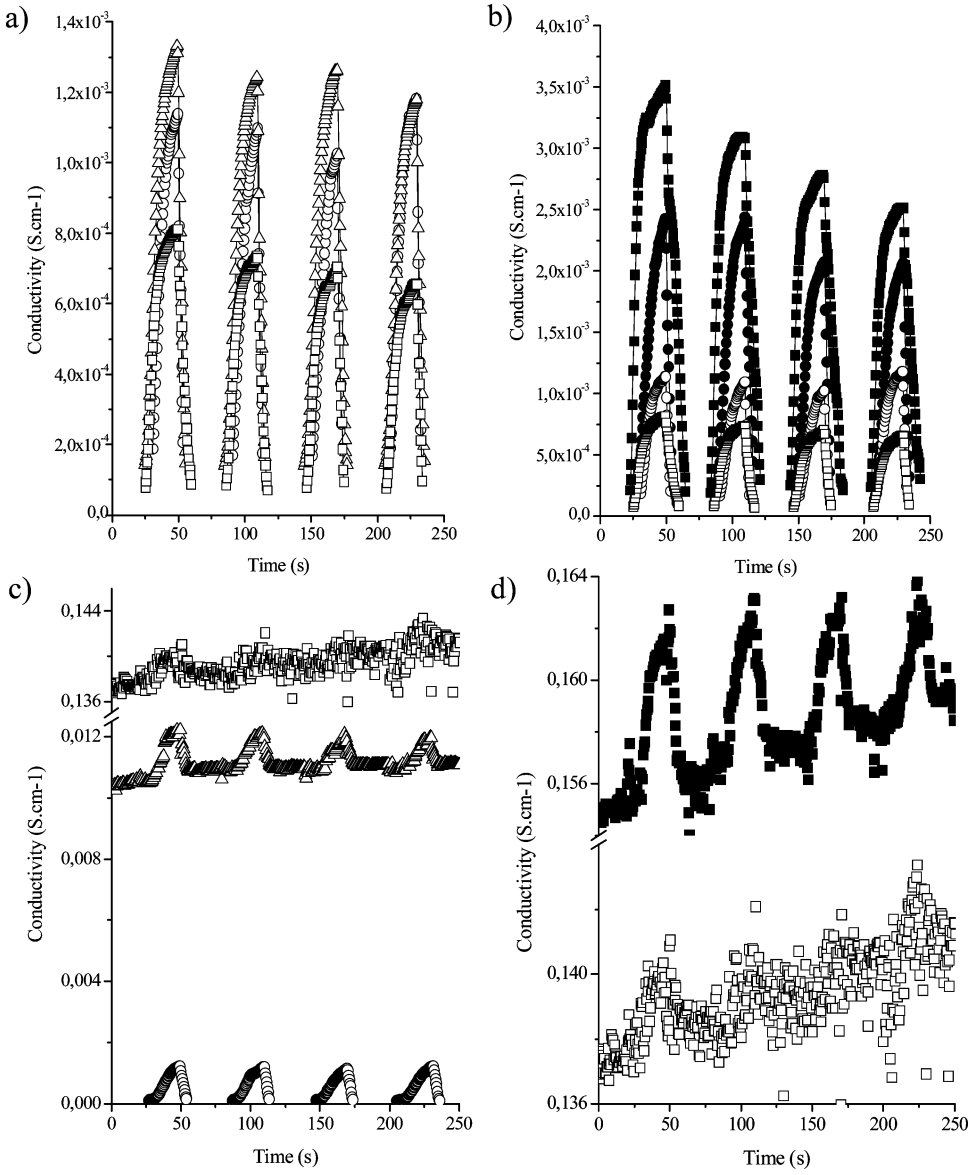

Figure 10. The provided results have been obtained for a single vanadium oxide fiber. (a) Latex contents at a constant shear rate $\dot{\gamma}$ equal to -158 s^{-1}: ○, 10 wt % latex; △, 30 wt % latex; □, 60 wt % latex. (b) Effect of shear rates and latex contents: ○, 10 wt % latex and $\dot{\gamma}$ equal to -158 s^{-1}; ●, 10 wt % latex and $\dot{\gamma}$ equal to 235 s^{-1}; □, 60 wt % latex and $\dot{\gamma}$ equal to -158 s^{-1}; ■, 60 wt % latex and $\dot{\gamma}$ equal to 235 s^{-1}. (c) Effect of latex contents over calcined fibers at a constant shear rate $\dot{\gamma}$ equal to -158 s^{-1}: ○, 10 wt % latex; △, 30 wt % latex; □, 60 wt % latex. (d) Effect of shear rates over calcined fibers: □, 60 wt % latex and $\dot{\gamma}$ equal to -158 s^{-1}; ■, 60 wt % latex and $\dot{\gamma}$ equal to 235 s^{-1}.

the same than that observed for fibers free of latex contents, i.e., as the shear rate increases the Young's modulus is increasing while the plastic regime is minimized. Considering the uncalcined fibers, we observe an increase of the plastic regime of mechanical properties concomitant with a decrease of the Young's modulus as the latex content is increasing from 10 to 60 wt %. The appliance of a thermal treatment strongly decreases the mechanical properties of the as-synthesized porous vanadium oxide fibers. The sensing properties are strongly affected by the removal of the insulators PVA and latex contents by the applied thermal treatment, where the fibers' sensitivity is enhanced. If varying the porosity does not induce much fluctuation over the detection times (sensitivity), the fiber thermodynamic stabilities are strongly affected and increased with the induced porosity. On the other hand, we notice that the emerging porosity is a strong penalty toward the sensing-cycling properties of the final porous vanadium oxide fibers. Overall, the conclusion is that all the parameters involved within the mechanical and sensing properties are not acting within a cooperative fashion but rather in a strong partitive one. For instance, if we increase the fibers sensitivity with the removal of PVA and latex, on one hand, we will increase the fiber thermodynamic stability, but on the other hand, the fiber mechanical and cycling properties will be strongly diminished.

Taking into account the strong partitive action mode of the applied shear rates, organic contents, and induced porosity, this work reveals that the intrinsic fibers outer surface conductivity is a key factor for the sensing property and that the effect of varying the porosity, if not obvious for the sensing aspect, is appearing as an important parameter for the thermodynamic stability. But at that stage, if the effect

of porosity is optimizing the fibers thermodynamic stability, both cycling and mechanical properties are inhibited. Considering this conclusion, a nice way to promote and enhance both the fiber sensing and mechanical properties would be to generate an extrinsic plasticity associated with an intrinsic enhanced conductivity. Regarding this issue, we intend to design composite fibers made of vanadium oxide and polyaniline. This work is under way and will be published in due time.

Acknowledgment. This work is part of the European FAME-MIOH 6th PCRDT program. We would like to acknowledge the "Region Ile-de-France" for financial support (grant E.1663)

Supporting Information Available: ESR spectrum of the as-synthesized V_2O_5 fibers recorded at room temperature (PDF). This material is available free of charge via the Internet at http://pubs.acs.org.

CM0711966